inorganics

MDPI

Article

A Simple Method to Obtain Protective Film against Acid Rain

Ana-Maria Mocioiu [1], Diana-Irinel Băilă [2], Cosmin Iulian Codrea [3,4] and Oana Cătălina Mocioiu [4,*]

[1] National R&D Institute for Non-Ferrous and Rare Metals, Biruinţei Blv. 102, Pantelimon, 077145 Ilfov, Romania; ammocioiu@imnr.ro
[2] Faculty of Industrial Engineering and Robotics, Polytechnic University of Bucharest, Splaiul Independentei No. 313, 060042 Bucharest, Romania; diana.baila@upb.ro
[3] Faculty of Applied Chemistry and Materials Science, Polytechnic University of Bucharest, Splaiul Independentei No. 313, 060042 Bucharest, Romania; ccodrea@icf.ro
[4] Institute of Physical Chemistry Ilie Murgulescu of the Romanian Academy, Splaiul Independenţei No. 202, 060021 Bucharest, Romania
* Correspondence: omocioiu@icf.ro

Abstract: Acid rain is a major problem for animals, plants, buildings, and also for the top glass of photovoltaic (PV) solar panels and greenhouses. Air pollutants such as NOx, NH_3, and H_2S can mix with water in the atmosphere to form acid rain. It was discovered that atmospheric water vapor adsorbed on the surface of glass can also lead to corrosion of the glass surface. The purpose of this work is to obtain a protective film for glasses used in different domains such as solar cells, windows, stained glass windows from historical buildings, etc. Thin film deposited on glass must be protective against acid rain, transparent in the visible domain with a band gap up to 3.2 eV, and have a vitreous structure (glass). Electron beam (e-gun) technology is a deposition technique for producing high-purity and dense coatings in a short time. It is well known that Ta_2O_5 is an oxide with anticorrosive properties, but it is expensive and cannot form glass by itself. ZnO is an oxide known as a glass former, exhibiting good optical properties. In this paper, a thin film obtained by the deposition of ZnO and Ta_2O_5 on a glass substrate using e-gun technology are studied. The simulated acid rain effect on the structure, morphology, and optical properties of thin films are studied after a 65% nitric acid attack on the surface. The X-ray diffraction (XRD) pattern shows the vitreous state of the thin film with a composition 50%ZnO 50%Ta_2O_5 before and after the acid attack. The morphology, composition, and thickness of the film are investigated using scanning electron microscopy with energy dispersive spectroscopy (SEM/EDS) and profilometry.

Keywords: ZnO; Ta_2O_5; thin film; corrosion

Citation: Mocioiu, A.-M.; Băilă, D.-I.; Codrea, C.I.; Mocioiu, O.C. A Simple Method to Obtain Protective Film against Acid Rain. *Inorganics* **2022**, *10*, 44. https://doi.org/10.3390/inorganics10040044

Academic Editor: Christian Julien

Received: 9 February 2022
Accepted: 29 March 2022
Published: 31 March 2022

1. Introduction

Acid rain is a major problem for animals, plants, buildings, and also for the top glass of photovoltaic (PV) solar panels and greenhouses [1–22]. Acid rain is considered one of the most dangerous factors of local pollution. This rain possesses higher levels of hydrogen ions (H^+) because of the contamination of sulfuric and nitric acids. Northeast America (Menz, Seip, 2004), Central Europe (Ilomuanya 2019, Menz, Seip, 2004), Malaysia (Omar, Rindam 2011), and China (Zhang 2017) have been identified as the largest acid rain affected regions in the world [1–8].

The pollutants from air such as NOx, NH_3, and H_2S can mix with water from atmosphere to form acid rain [1]. The pH of water is neutral (pH 6–7). Generally, any rain with a pH below six is considered acid rain. For example, the pH value of lemon juice is two, and the pH of vinegar is three. Typical pH values of acid rain for anthropogenic emissions may be in the range of 3.5–5 (Kim et al., 2007) [1,2]. Water with a pH of 4 is about 20 times more acidic than normal rain.

Acid rain not only damages the natural ecosystem, but also man-made materials [1–24]. Buildings, streets, outdoor sculptures, glass isolators for electric field distribution, etc.

have been subject to attack by weathering: sun, wind, frost, and the effects of rain [1–24]. Acid rain can accelerate the rate of this damage. Sometimes, acid rain is called "the unseen plague" [1]. The effects of acid rain must be reduced for the welfare of the global ecosystem [1].

The influence of different types of acid rain (sulfuric acid type acid rain, nitric acid type acid rain, and mixed type acid rain) on the stability of semi-flexible pavement, have been reported [7].

Du (2020) studied the effects of mixed acid rain with different molar ratios of SO_4^{2-} and NO_3^- (0:1, 1:0, 2:1, 1:1, and 1:2) on stream leaf breakdown through a microcosm experiment [10]. A significant inhibition of leaf breakdown rate was observed when the ratio was 1:2, with reduced microcosm pH, fungal biomass, and enzyme activities, as well as the frequencies of hub generally found in the fungal community [10].

Du (2022) showed the combined effects of acid rain and ZnO nanoparticles on plant litter decomposition through a microcosm experiment [8]. The decomposition rate of plant litter was increased by 123–204% by co-exposures [8].

Livingston [11] reported that acid rain damages the cultural heritage, particularly outdoor marble and bronze sculptures. This study involved the development of pH vs. SO_4^{2-} phase diagrams for marble (calcium carbonate) and bronze (copper-tin) under ambient conditions [11]. They used modeling of the acid neutralization for pH in the 3.5–6 range typical in wet deposition [11]. In the case of marble, the theoretical results for Ca^{2+} ions lost due to acid rain neutralization is 0.158 mmol/L compared to 10.5 mmol/L by dry deposition. For bronze, the Cu^{2+} ion losses are theoretically 0.21 mmol/L and practically 47.3 mmol/L. Therefore, dry deposition effects have the potential to dominate over wet deposition effects [11].

Most of the historic buildings in Malaysia commonly use building materials such as (1) timber, (2) stone, (3) brick, and (4) plaster in their construction [5]. Acid rain is characterized as erosive and decolorate. It impacts construction materials like iron, zinc roofing, and limestone [5]. Acid rain causes the discoloration of paint and rocks such as limestone, reducing the aesthetical value of buildings and bridges [5]. An analysis of the status of acid deposition has shown some slight variation in pH values of the rainfall between regions in Malaysia [5]. The pH level of rain was between 4.2 and 4.4 [5].

Medieval stained-glass windows constitute a part of cultural heritage that has been exposed to environmental damage over centuries [12]. This provides an exceptional opportunity to analyze the durability of glass and to identify the long-term environmental corrosion processes on glass [12]. In the case of historic buildings, both rocks and glasses have been exposed to the same atmospheric conditions, which allows for a comparison of the corrosion mechanisms on both materials [12]. Medieval stained glass (13th–15th centuries) from three restoration works (the Santa Maria del Mar and the Pedralbes Monastery church in Barcelona, and the Tarragona Cathedral in the northwestern Mediterranean Region) have been studied to characterize glass decay [12]. The stained-glass windows were built around 1330, and since that time, the monastery and church have been under the auspices of the Barcelona municipality. There are very well-preserved sets of stained glass with exceptional preservation of original glass pieces in their medieval lead frameworks [12]. Over the centuries, later damage and repairs have led to a mixture of old glass panels with new ones, the most important modifications probably dating from 1808 and 1939 [12]. The windows show original black-fired designs [12]. Electron microprobe analysis provided evidence of two types of glass: an Na-rich type (stable, Mediterranean, of Roman-like tradition), and a K-Ca-rich type, similar to coeval Central European medieval stained glasses [12]. The defects defined as destructive (micro- and meso-pitting) and constructive (patina and micro-crust) were observed the on glass surfaces [12]. This type of decay in the K-Ca-rich glasses is in terms of thickness reduction in flat glass was at an order of magnitude less than that that commonly found in Central European countries with a continental climate [12]. Macroscopic and microstructural studies allowed for the identification of biodeterioration decay, with chemical effects similar to those for pure

chemical hydration leaching and corrosion, associated with biomineralization by unspecific sulfate (gypsum, syngenite) and calcite mineralization, as well as bio-induced (weddellite, whewellite, etc.) mineralization [12]. The authors established the following succession of bands from unaltered glass to the surface: a gel-like hydrated silica glass (depleted in most elements), beige-orange patina, and a sulfate weathering crust mostly consisting of gypsum and, locally, with interstitial K-Ca (syngenite) or K-Mg sulfates [12]. Some extreme pathologies such as dramatic thinning of glass pieces, significant physical decay, and the development of generalized corrosions and associated thick crusts are absent. Several factors can be invoked to explain this. Widespread use of Na-rich glass, characterized by silica contents around 60% in weight, is a primary factor that explains the good preservation of these stained-glass pieces; the role of silica as a network-forming agent has also been clearly shown [12]. Therefore, it seems useful to concentrate on the K-rich glasses present in the same windows to determine if the decay processes and pathologies are comparable to those described for Central European medieval windows. The lesser degree of decay in the Mediterranean Region can be interpreted in terms of different stages of the same processes [12]. This implies that differences in decay are related to different kinetics of similar processes related to the same agents [12]. The basic chemistry of the process of stained-glass decay is well known: first, attack by water allows for the formation of hydroxides, cation migration, and loss of a superficial film by leaching and hydration. Next, the subsequent conversion of these hydroxides to carbonates by carbon dioxide in the atmosphere takes place, and finally, the conversion of those carbonates to sulfates occurs [12]. During this process, the surface of the glass can develop several microchemical environments from case to case, as a function of the different chemistry of stained glasses [12]. It is not easy to quantify the decay in medieval stained glasses, since they do not display a homogeneous thickness as does industrial glass [12]. The measured thickness of the K and K-Ca glasses is around 2–3 mm on average, while Na glass can be thicker (3 to 4 mm) [12]. The authors concluded that the decay effects are on around 20 to 30 times greater for glasses in continental climates with an Atlantic influence where the mean rainfall is in the range of 750–900 mm/year [12].

While the issue of maintenance has been highlighted, building and stained-glass window conservation should also be taken into consideration.

A sustainable and green energy supply is required for human life and the economic development of populations all over the world. Photovoltaic (PV) materials convert sunlight into electrical energy. A single PV device is known as a solar cell. The life of solar cell operation is about 10 years. Thin-film solar cells are of great interest because of their high-cost effectiveness as compared with monocrystalline cells [9]. PV solar cells suffer from a loss in efficiency due to corrosion of the top glass [9]. The top glasses used for solar cells are borosilicate or soda-lime glasses. They are characterized by high optical transmittance at low cost [9]. It was discovered that atmospheric water vapor adsorbed on the glass surface can lead to corrosion of the glass surface [11–24]. The chemical resistance of glass is conventionally designated as the opposition of the glass subjected to attack from aqueous solutions and atmospheric agents (water vapor, CO_2, NOx, SO_2) [9,23,24]. Depending on the region of the world, the acid rain can contain sulfuric acid (H_2SO_4), nitric acid (HNO_3), and carbonic acid(H_2CO_3) in different concentrations. The alteration of glass is based on its reaction with adsorbed or condensate water. Such corrosion is not as effective, but becomes much stronger under the action of temperature (60–90 °C). The solar cells working temperature is 100 °C. The top glasses of solar cells are materials resistant to weak acids, and the greatest damage is done by nitric acid.

The formation of nitric acid from gases and rain is shown in the following reactions:

$$NO(g) + OH^- \rightarrow HNO_2\ (aq)$$
$$NO_2(g) + OH^- \rightarrow HNO_3\ (aq)$$

Using the isotopic water vapor ($H_2{}^{18}O$) for hydration experiments performed at 90 °C, Kudriavtsev (2019) demonstrated that the interaction between water vapor and borosilicate

differed from the interaction between water vapor and soda-lime glass [9]. In the first case, the formation of a hydrogenated layer was observed over time, due to the reaction of water with the glass network only at the surface and subsequent reactions between protons and glass modifiers (oxides of trivalent metals) with the formation of hydroxides [9]. The water vapor adsorbed on the surface of soda-lime glass resulted in the ion-exchange reaction between H and alkali metals (Na, K) in the glass, with the formation of a hydrated layer that grew with time [9].

When the glass surface is in contact with an aqueous acidic medium, the H+ ions of the medium can replace alkaline and transitional atoms (M) from the glass surface [9,23].

$$\text{Si-O-M-O—Si} + 2H^+ \rightarrow 2(\text{Si-O-H}) + M^{2+}$$
$$\text{Si-O-M} + H^+ \rightarrow \text{Si-O-H} + M^+$$

An experiment to simulate the real process of solar cell glass superstrate corrosion occurring in open air was conducted using the hydration of borosilicate glass in water vapor with 100% humidity at 88 °C over a period of two months [9]. When water molecules penetrate into the soda-lime silicate glass, sodium and potassium leave the near surface layer and form a "sediment layer" of alkali salts on the surface [9]. In the case of glass hydration in water, the alkalis dissolve in water, leaving the surface unpolluted [9]. In the case of borosilicate glass, the transmittance decreased insignificantly during the hydration experiment [9]. The difference in the observed effects of corrosion can be explained by the difference in the mechanisms of the water vapor–glass surface interactions in those glasses [9]. It is important to notice that the water vapor–glass interaction differs significantly from the water–glass interaction [9]. The authors observed a strong participation of alkali metals in the glass corrosion process for both types of glasses [9]. For the alkali-free borosilicate glass Corning 1737 hydrated under the same conditions and during the same period, neither hydration nor hydrogenation can be observed [9]. Thus, alkali-free glasses should be used for photovoltaic applications [9].

In order to protect glass surface against acid rain, thin films with chosen compositions and anticorrosive properties can be deposited on glass using different methods.

It is well known that Ta_2O_5 is an oxide with anticorrosive properties, but it is expensive and cannot form glass by itself. ZnO is an oxide known as a glass former and exhibiting good optical properties.

The literature reports the use of crystalline ZnO films, amorphous and crystalline Ta_2O_5 films, Zn doped Ta_2O_5 films, ZnO/Ta_2O_5 successive crystalline films, and ZnO-Ta_2O_5 deposited on alloys with Co-Cr support [23–33].

Electron beam technology (e-gun) is a deposition technique for producing high-purity coatings in a short time [29,30]. The advantages are as follows: (1) the e-beam source is capable of heating oxides to high temperatures (up to 3000 °C); (2) films deposited by electron beam evaporation can maintain the purity of the oxide; (3) source and support types can be created in a variety of sizes. This method uses vacuum at a pressure of 10^{-5} to 10^{-6} torr. The most common technologies for physical deposition are PVD and sputtering [21,25,26,28–33]. The angle of incidence flux influences the properties of the film. The quartz crystal microbalance controls the coating growth, reporting the thickness and evaporation rate.

Corbella studied thin films of Ta_2O_5 deposited by RF-magnetron reactive sputtering from a tantalum oxide target [26]. Fused silica, alumina glasses, and WO_3/ITO on glass were used as substrates. The amorphous optical band gap energy values ranged between 4.10 and 4.25 eV [26]. The variation of the process parameters leads to the possibility of using these films as solid electrolytes for electrochromic devices built on glass substrates [26].

Ta_2O_5/ZnO heterojunction for metal-oxide-semiconductor (MOS) structured devices was fabricated by using radio-frequency magnetron sputtering and ion beam sputtering technologies on a α-sapphire substrate [27]. The band alignments of ZnO with other oxides are the key issues for predicting its interface behaviors and determining the carrier [27]. The reported band gap values are 3.97 eV for Ta_2O_5, 3.26 eV for ZnO, the conduction band

offset is 0.33 ± 0.03 eV, and valence band offset is 0.38 ± 0.03 eV, indicating a type I band alignment [27].

Physical vapor deposition (PVD) or chemical vapor deposition (CVD) lead to films that have an amorphous phase (a-Ta_2O_5), or two distinct crystal phases depending on the annealing, that is, an orthorhombic b-Ta_2O_5 and a hexagonal d-Ta_2O_5 [28]. Sputtered films are smooth and of good structural quality and uniform thickness [28]. A test film annealed in air at 800 °C for 1 h yielded well-defined XRD patterns. The samples become nanocrystalline, with a dominant orthorhombic phase (JCPDS: 25-0922) [28]. Thermal stresses in the thicker samples after annealing were significant enough to cause cracking, and this effect contributes to volume scattering in the sample, thus affecting the near-IR transmittance [28].

Ta_2O_5 and ZnO thin films deposited by e-gun technology on Co-Cr alloy disks manufactured by Direct Metal Laser Sintering were studied for dental crowns and implants [29]. The Co-Cr alloy was thermally treated in a furnace for 30 min at 900 °C [29,30]. The films obtained were crystalline, with nano-particles between 11 and 25 nm [29]. The best thin film (Ta_2O_5 (50%) and ZnO (50%)) for dental applications presented uniform grains, having the diameter of the nanometer order [29].

The literature data reported a band gap of 4.18 eV for Ta_2O_5 films [31] and 3.25 eV for ZnO [27,32]. Ta_2O_5 is an interesting material with a very high refractive index ($n \approx 2.2$, $\lambda = 633$ nm), a wide band gap (Eg = 4.2 eV), and a transparent nature in a wide wavelength range from 300 nm to 2 µm [32].

ZnO-doped tantalum oxide films (doping concentration 0, 1, 3, and 5 wt.%) have been prepared using a pulsed laser deposition technique in a reactive oxygen atmosphere, and the films are annealed at temperatures of 973 and 1173 K [33]. XRD analysis shows that the ZnO-doped films annealed at 973 K are crystalline in nature; whereas, the annealed counterpart of pure Ta_2O_5 is amorphous. On annealing at 1173 K, the undoped film shows good crystallinity; whereas, the ZnO doped film presents a decline in crystallinity compared to that of the films annealed at a temperature of 973 K [33]. Ta_2O_5 nanoring of diameters around 700 nm have been observed in the AFM micrographs of 3 wt.% and 5 wt.% ZnO-doped Ta_2O_5 films [33]. The band gap increases with increasing ZnO doping and increasing treatment temperature.

The purpose of this article is to obtain a thin film for the top glass of the solar cells in order to be protective against simulated acid rain on a vitreous structure (glass). The film must be transparent in the visible range and must have a band gap up to 3.2 eV. The e-gun technology is used to obtain a thin film, with anticorrosive and optical properties, on a borosilicate glass substrate.

2. Materials and Methods

The chemical composition of the borosilicate glass substrate is SiO_2 69.13%; B_2O_3 10.75%; BaO 3.07%; Na_2O 10.40%; K_2O 6.29%; As_2O_3 0.36%. The glass substrate contains class 2 hydrolytic resistance, according to the literature. The borosilicate glass substrates from Schott Company are first cleaned with ethylic alcohol, and then plasma glow discharges at 200 mA, 6 Pa, 2500 V. Zinc oxide, CAS No. 1314-13-2, from Sigma-Aldrich (St. Louis, MO, USA), and tantalum (V) oxide with a purity of 99%, CAS No. 1314-61-0, from Sigma-Aldrich (St. Louis, MO, USA) are used as raw materials. The thin film deposition was similar to that reported previously for coating of the Co-Cr alloy [29,30]. The deposition process is achieved using the base pressure in the high vacuum range to minimize the interactions number between the evaporate particles and the residual gases in the chamber. The high vacuum allows for the particles to have a "mean free path" for the thin film deposition at the substrate. The coating growth controller is a quartz crystal microbalance, which determinates the thickness and evaporation rate. The PVD evaporation chamber is equipped with two e-guns, one for Ta_2O_5 and the other for ZnO, in order to diminish contamination. Both oxides are vaporized thermally to 3000 °C. The important parameters of this technology are the speed of the evaporated particles, between 1 and

3 nm/s, and the angular distribution of 180 degrees. Baila [29] obtained nanocrystalline ZnO-Ta_2O_5 films on a Co-Cr alloy due to metallic support. In this paper, the structure of the deposited films is determined by X-ray diffraction (XRD) scans using the Ultima IV X-ray Diffractometer (Rigaku, Tokyo, Japan), Cu Kα radiation. The thin film of composition of 50 mol% ZnO 50 mol% Ta_2O_5 was the only one with a vitreous structure. In order to simulate the action of acid rain on the surface of thin films, corrosion with 65% nitric acid for 2 hours (PH = 1) is performed. In our example, when pH is 1, this simulates the action of acid rain for more than 10 years. The analysis of the film surface morphology and composition was performed by scanning electron microscopy with energy dispersive spectroscopy (SEM/EDS) using the FEI Quanta 250 model, operating at 10 kV in high vacuum mode. The glass coated with the thin film was immobilized on a double-sided carbon tape, with no coating. The Profilm 3D (Filmetrics, San Diego, CA, USA) optical profilometer with White Light Interferometry (WLI) is used for topographic analyses. The performance specifications in measuring the surface profiles include a step height accuracy of 0.7% and a thickness range of 50 nm to 10 mm. The images have been processed with Profilm Software (Filmetrics, San Diego, CA, USA). Note that the scale will automatically adjust to match the length of the segment in the diagonal mode. The graph updates to scale based on the length of the line. The optical properties are obtained from the spectra recorded on a Cary 100 UV-Visible Spectrophotometer; in the range of 800–200 nm.

3. Results

Figure 1 presents the XRD patterns of the glass substrate, glass coated with thin film, before and after acid corrosion. The possible applications as a protective film for the top glass of solar cells or as a protective film for windows require the vitreous state of the film. The thin film with a composition of 50%ZnO50%Ta_2O_5 was the one exhibiting a vitreous structure at a higher tantalum oxide content. All paterns show a wide peak characteristic of a vitreous state. After corrosion, the shape is not modified, which shows the good chemical resistance of the film to the corrosion of nitric acid 65%. In the case of low chemical resistance of the glasses after an acid attack on the surface, small crystallites or other compounds appear that can be observed in the XRD diagrams. The absence of salts or other compounds on the glass surface provide for a good optical transmittance.

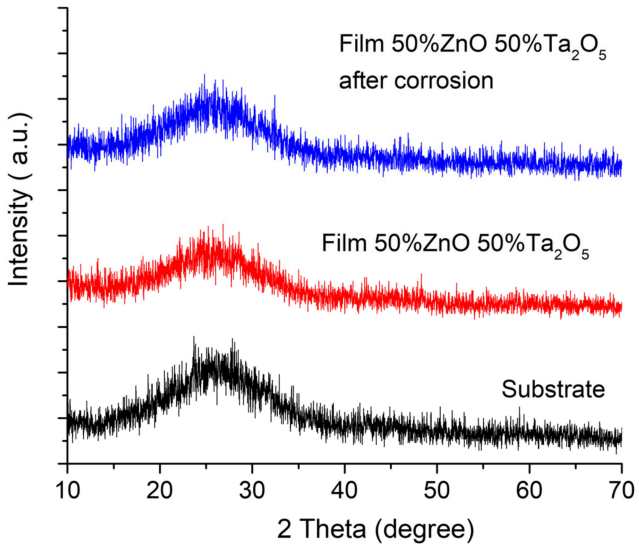

Figure 1. XRD patterns of the substrate 50%ZnO50%Ta_2O_5 film before and after corrosion.

Figure 2 shows the SEM image and EDS spectrum of the 50%ZnO50%Ta_2O_5 film deposited on a borosilicate glass support using e-gun technology.

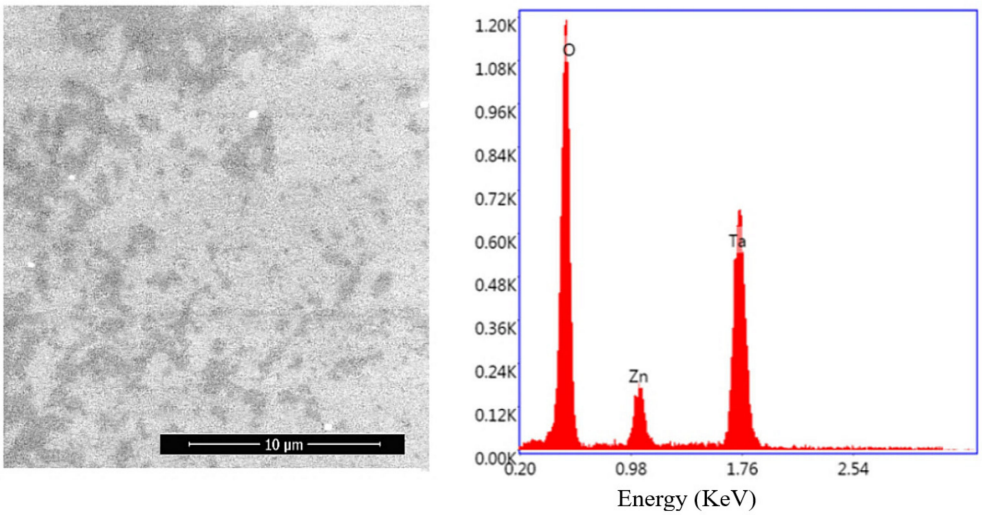

Figure 2. SEM/EDS images of 50%ZnO50%Ta_2O_5 film deposited on borosilicate glass.

The images of the film at a magnification of 10,000× show a glassy aspect of the surface, without particles. The images show darker areas—probably richer in tantalum oxide—and lighter areas—probably higher in zinc oxide.

The EDS data from confirm the composition of the film. The elemental analysis provides the following results: 47.74 wt.% OK, 9.54 wt.% ZnL, 42.72 wt.% TaM.

Figures 3 and 4 show the topographic profile created on the surface using optical profilometry measurements.

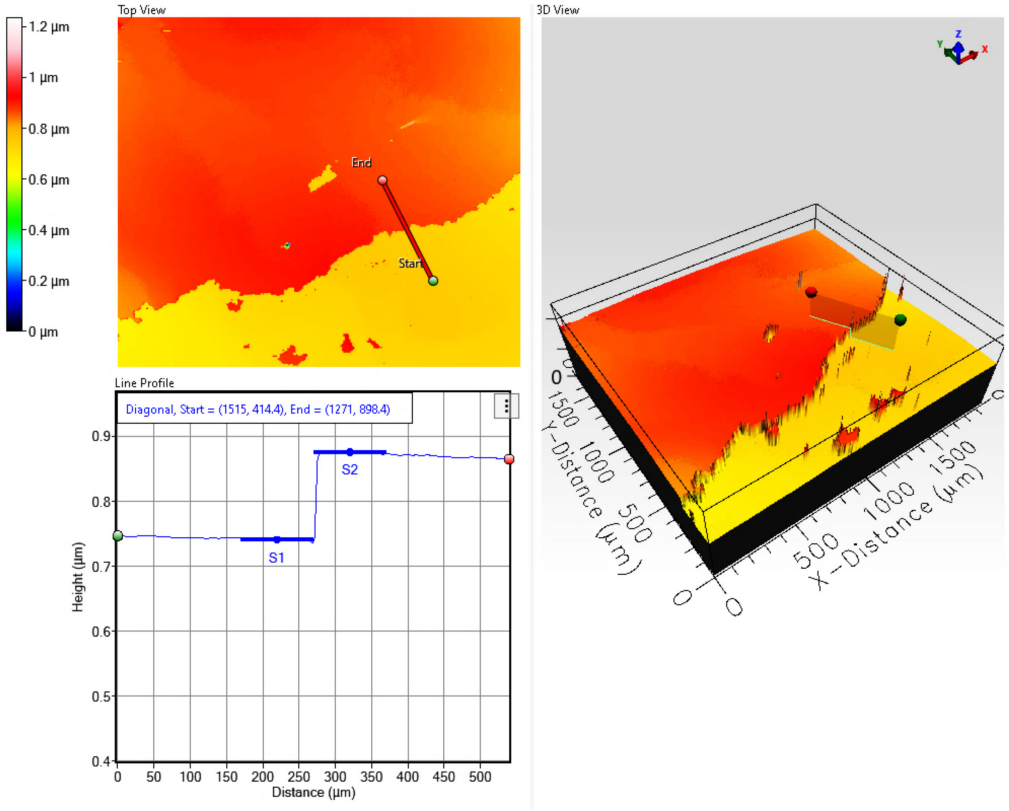

Figure 3. Surface profile and thickness of 50%ZnO50%Ta_2O_5 film deposited on glass.

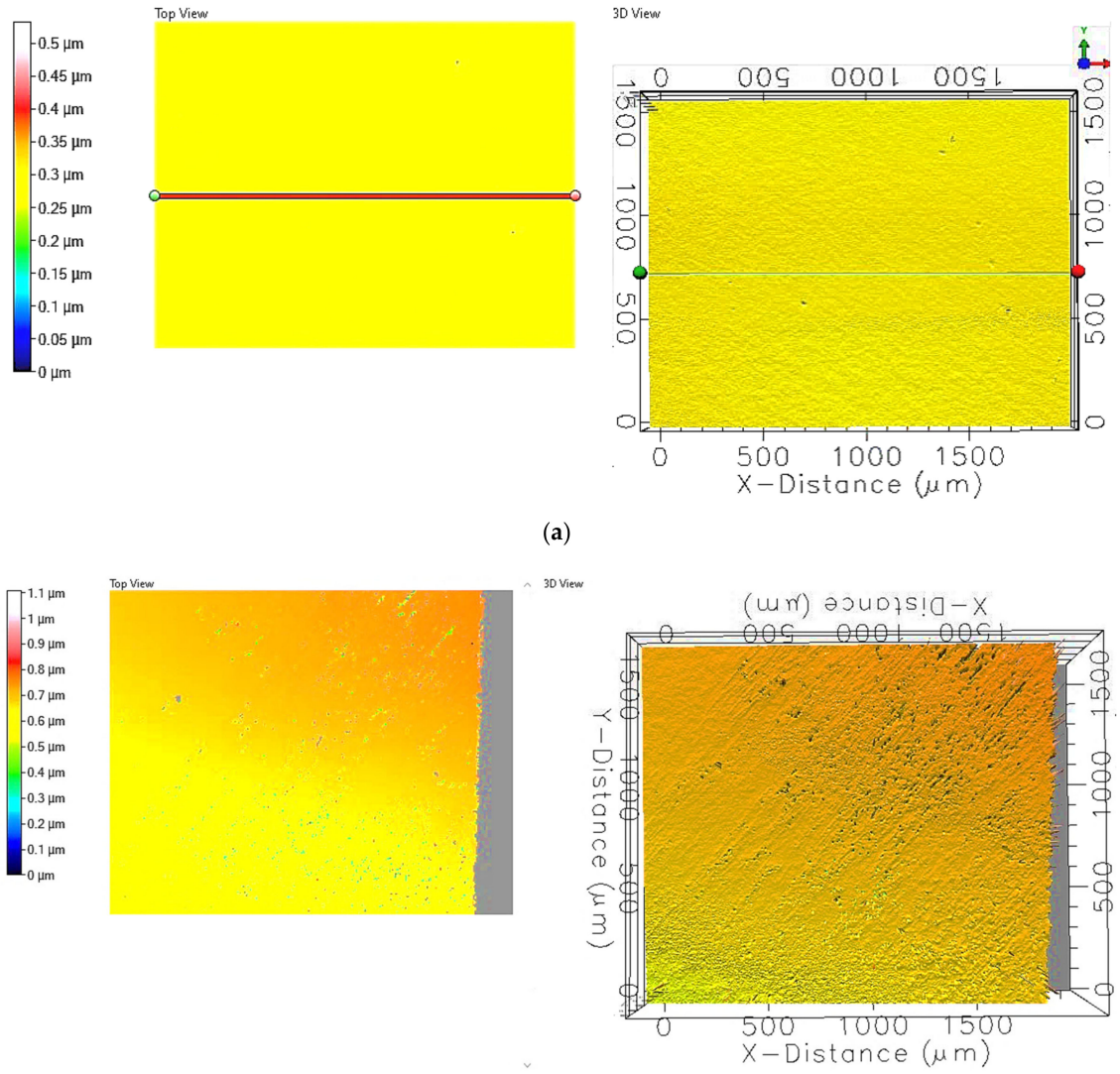

Figure 4. Surface of 50%ZnO50%Ta_2O_5 thin film (**a**) before and (**b**) after corrosion in nitric acid.

The film was investigated using wide area film surface topography, and profiles were mapped by the white light interferometry technique using a Filmetrics Profilm 3D optical profiler. By analyzing the 2D and 3D image obtained, along with the color scale, it is shown that the film roughness is 1.6 nm and the thickness is 131 nm. After corrosion, the surface of the thin film presents small holes, as can be seen in Figure 4. The film roughness increased to 3.9 nm, and the thickness decreased to 107 nm. The image of the film after corrosion shows small defects on the surface, along with an increased roughness.

Figure 5 shows the UV-Vis spectra measured for the borosilicate glass substrate and 50%ZnO50%Ta_2O_5 film before and after corrosion. In the visible region between 380 nm and 800 nm, the optical transmittance of the films is above 75%, which means that these films are transparent. The optical transmittance varies from ~75 to 95% due to the thin film interference effects resulting from the overlaying of light reflected on both sides of the thin film [31]. The maximum and minima on the spectra come from the constructive and destructive interference effects. Within a fixed wavelength range, the numbers of both maxima and minima on each spectrum depend on the optical thickness [31]. In the case of the thin film, the transmittance decreases insignificantly during the corrosion experiment. The transmission decreases a bit in the lower wavelength region, possibly due to absorption

caused by oxygen deficiency or a lack of ion assistance during thin film growth. In the UV region, below 380 nm, a sharp decrease in optical transmittance occurs. This behaviour can be explained due to substrate absorption in the UV region and to the heavy absorption of light that is generally associated with the optical transitions through the energy gap of tantalum oxide [31]. The thin film bands move to a lower wavelength in the ultraviolet region, from 250 nm to 240 nm, and to a higher wavelength in the visible region, from 585 nm to 685 nm. The results from UV-VIS can be correlated with data obtained from the profilometer, and the changes in the optical spectrum can be explained by an increased roughness at the surface of the film after corrosion.

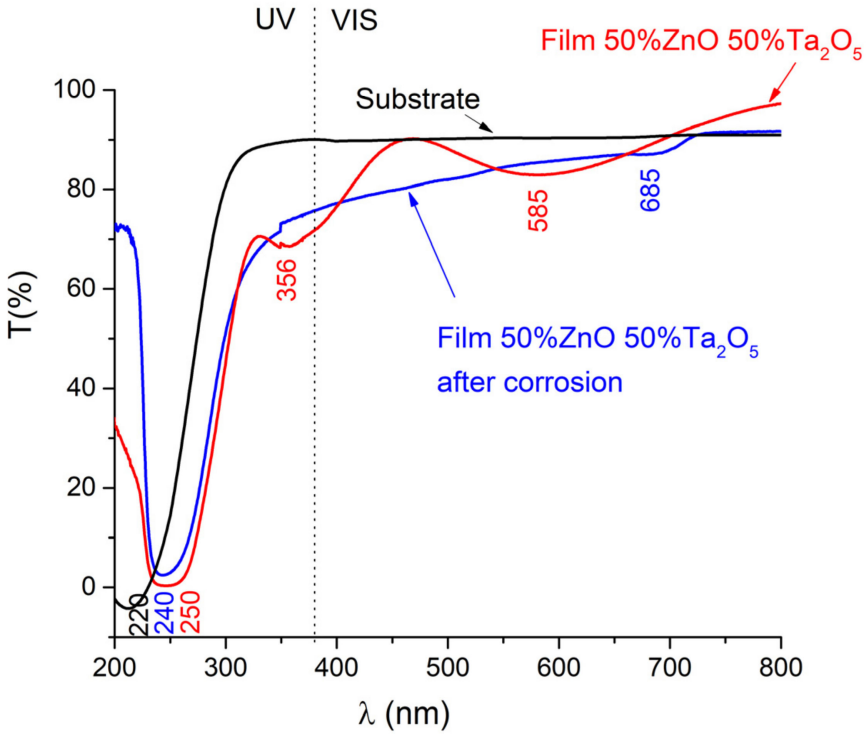

Figure 5. UV-VIS spectra of the substrate and film 50%ZnO50%Ta_2O_5 before and after corrosion.

The optical direct band gap of the thin film is calculated according to the methods outlined in the literature [31,32]. When the thin film is non-crystalline, Tauc plots can be used to determine the optical direct band gap. Figure 6 presents the Tauc plot $(\alpha h\nu)^2$ vs. energy ($h\nu$) for the film before and after corrosion. The band gap value is obtained from the intersection of the tangent of the absorption edge (straight line in the graph) with the *x*-axis.

The formulas used for axes of Tauc plot are:

$$h\nu = hc/\lambda = 1240/\lambda$$
$$\alpha = -\ln(T)/t$$

where α is the linear absorption coefficient and t is the film thickness.

The optical direct band gap of the thin film was 3.9 eV for the 50%ZnO50%Ta_2O_5 film before corrosion and 3.7 eV after corrosion. The film exhibits a better band gap than ZnO and is obtained at a lower cost than the Ta_2O_5 film. The thin film can be used for the protection of solar cells due to the band gap above 3.2 eV. Due to its high transmittance, the thin film can also be used to protect historical glass windows.

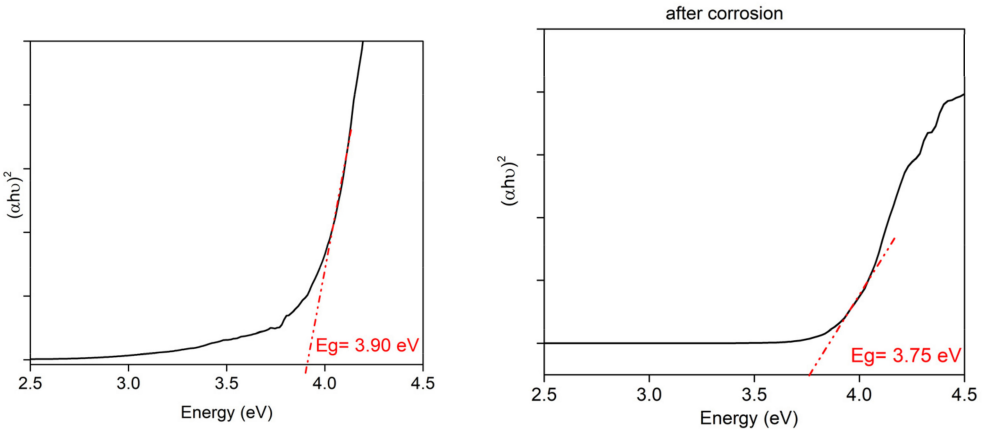

(**a**) (**b**)

Figure 6. Tauc plot for band gap (Eg) determination of the 50%ZnO50%Ta_2O_5 thin film (**a**) before and (**b**) after corrosion.

4. Conclusions

The thin film with a composition of 50%ZnO50%Ta_2O_5 and a thickness of 131 nm was obtained using e-gun technology. The glass substrate and composition were important in obtaining the vitreous state of the thin film. The thickness and roughness of the film are at appropriate parameters for the desired applications. A corrosion test similar to the acid rain effect was applied. The 50%ZnO 50%Ta_2O_5 thin film exhibits good optical and anticorrosive properties, determined from the UV-Vis spectra and XRD patterns. Corrosion insignificantly decreases the transmittance in the visible region, meaning that the film thickness decreases, but it is not dissolved. The thin film shows a transmittance in the visible region above 75% and a band gap of 3.9 eV. The band gap value indicated for the top glass of solar cells must be above 3.2 eV. The thickness and the chemical composition (especially the ZnO constituent) of the film are important and lead to low economic costs. Due to its high transmittance, the 50%ZnO50%Ta_2O_5 film can be used to protect historical windows or top glass of solar cells against the effects of acid rain.

Author Contributions: Conceptualization, writing, review and editing, A.-M.M. and O.C.M.; film deposition: D.-I.B.; formal analysis, A.-M.M., O.C.M.; profilometer measurements PhD student C.I.C. All authors have read and agreed to the published version of the manuscript.

Funding: This research received no external funding.

Informed Consent Statement: Not applicable.

Acknowledgments: The work of I. Atkinson in recording XRD pattern is acknowledged. The work was supported by Program 4: Materials Science and Advanced Characterization Methods, Theme: 4.11.33 Synthesis and Characterization of Vitreous and Crystalline Materials for Solar Cells from Institute of Physical Chemistry Ilie Murgulescu of the Romanian Academy. The work of the PhD student Cosmin Iulian Codrea was supported by the project ANTREPRENORDOC, in the framework of the Human Resources Development Operational Program 2014–2020, financed by the European Social Fund under the contract 36355/23.05.2019 HRD OP/380/6/13—SMIS Code: 123847.

Conflicts of Interest: The authors declare no conflict of interest.

References

1. Mohajan, H.K. Acid Rain is a Local Environment Pollution but Global Concern. *J. Anal. Chem.* **2018**, *3*, 47.
2. Kim, M.G.; Kim, O.J.; Lee, H.Y. A Case Study on Acid Rain over Jeju Island, Korea. *J. Clim. Res.* **2007**, *2*, 33.
3. Zhang, Y.L.; Li, Q.; Zhang, F.; Xie, G. Estimates of Economic Loss of Materials Caused by Acid Deposition in China. *Sustainability* **2017**, *9*, 1. [CrossRef]
4. Menz, F.C.; Seip, H.M. Acid Rain in Europe and the United States: An Update. *Environ. Sci. Policy* **2004**, *7*, 253. [CrossRef]

5. Omar, M.Z.; Rindam, M. The Impact of Acid Rain on Historical Buildings in Kuala Lumpur, Malaysia. *Des. Princ. Pract. Int. J.* **2011**, *5*, 176. [CrossRef]
6. Ilomuanya, C.S.; Nekahi, A.; Farokhi, S. Acid Rain Pollution Effect on the Electric Field Distribution of a Glass Insulator. In Proceedings of the IEEE International Conference on High Voltage Engineering and Application (ICHVE), Athens, Greece, 10–13 September 2018; p. 18469248. [CrossRef]
7. Hu, C.; Zhou, Z.; Chen, G. Effects of different types of acid rain on water stability of asphalt pavement. *Constr. Build. Mater.* **2022**, *322*, 126308. [CrossRef]
8. Du, J.; Qv, W.; Niu, Y.; Yuan, S.; Zhang, L.; Yang, H.; Zhang, Y. Co-exposures of acid rain and ZnO nanoparticles accelerate decomposition of aquatic leaf litter. *J. Hazard. Mater.* **2022**, *426*, 128141. [CrossRef]
9. Kudriavtsev, Y.; Hernandez, A.G.; Asomoza, R. Solar cell degradation caused by glass superstrate corrosion. *Sol. Energy* **2019**, *187*, 82. [CrossRef]
10. Du, J.; Qv, M.; Zhang, Y.; Cui, M.; Zhang, H. Simulated sulfuric and nitric acid rain inhibits leaf breakdown in streams: A microcosm study with artificial reconstituted fresh water. *Ecotoxicol. Environ. Saf.* **2020**, *196*, 110535. [CrossRef] [PubMed]
11. Livingston, R.A. Acid rain attack on outdoor sculpture in perspective. *Atmos. Environ.* **2016**, *146*, 332. [CrossRef]
12. Garcia-Vallès, M.; Gimeno-Torrente, D.; Martínez-Manent, S.; Fernández-Turiel, J.L. Medieval stained glass in a Mediterranean climate: Typology, weathering and glass decay, and associated biomineralization processes and products. *Am. Mineral.* **2003**, *88*, 1996. [CrossRef]
13. Lu, C.; Wang, W.; Zhou, Q.; Wei, S.; Wang, C. Mechanical behavior degradation of recycled aggregate concrete after simulated acid rain spraying. *J. Clean. Prod.* **2020**, *262*, 121237. [CrossRef]
14. Saygili, Y.; Stojanovic, M.; Flores-Díaz, N.; Zakeeruddin, S.M.; Vlachopoulos, N.; Grätzel, M.; Hagfeldt, A. Metal Coordination Complexes as Redox Mediators in Regenerative Dye-Sensitized Solar Cells. *Inorganics* **2019**, *7*, 30. [CrossRef]
15. Jiang, R.; Boschloo, G. The Effect of Illumination Direction and Temperature on Dye-Sensitized Solar Cells with Viscous Cobalt Complex-Based Electrolytes. *Inorganics* **2018**, *6*, 60. [CrossRef]
16. Liu, Y.X.; Wang, Y.; Wang, Q.; Pan, J.F.; Zhang, J. Simultaneous removal of NO and SO_2 using vacuum ultraviolet light (VUV)/heat/peroxymonosulfate (PMS). *Chemosphere* **2018**, *190*, 431–441. [CrossRef] [PubMed]
17. Mocioiu, O.C.; Atkinson, I.; Pandele, J.; Boroica, L.; Sava, B.; Mocioiu, A.M.; Zaharescu, M. Protective coatings for the silicate glasses containing Fe_2O_3. *Rev. Roum. Chim.* **2014**, *59*, 267–272.
18. Xu, M.X.; Wang, Y.H.; Geng, J.F.; Jing, D.W. Photodecomposition of NOx on Ag/TiO_2 composite catalysts in a gas phase reactor. *Chem. Eng. J.* **2017**, *307*, 181–188. [CrossRef]
19. Kim, K.J.; Ahn, H.G. The effect of pore structure of zeolite on the adsorption of VOCs and their desorption properties by microwave heating. *Microporous Mesoporous Mater.* **2012**, *152*, 78–83. [CrossRef]
20. Ma, J.; Wang, C.; He, H. Enhanced photocatalytic oxidation of NO over g-C_3N_4-TiO_2 under UV and visible light. *Appl. Catal. B* **2016**, *184*, 28–34. [CrossRef]
21. Feng, F.; Yang, W.; Gao, S.; Sun, C.; Li, Q. Post illumination activity in a single phase photocatalyst of Mo-doped TiO_2 nanotube array from its photocatalytic "memory". *ACS Sustain. Chem. Eng.* **2018**, *6*, 6166–6174. [CrossRef]
22. Kaky, K.M.; Lakshminarayana, G.; Baki, S.O.; Kityk, I.V.; Taufiq-Yap, Y.H.; Mahdi, M.A. Structural, thermal and optical absorption features of heavy metal oxides doped tellurite rich glasses. *Results Phys.* **2017**, *7*, 166–174. [CrossRef]
23. Mocioiu, O.C.; Atkinson, I.; Cusu-Pandele, J.; Bratan, V.; Petrescu, S.; Baila, D.I.; Mocioiu, A.M. Structural and physico-chemical characterization of Zn-doped SiO_2 glasses obtained by sol-gel route. *Rev. Roum. Chim.* **2018**, *63*, 419–424.
24. Mocioiu, O.C.; Mocioiu, A.M.; Marin, A.; Zaharescu, M. Study of historical lead silicate glasses and their preservation by silica coating. *Ceram. Int.* **2017**, *43*, 77–83. [CrossRef]
25. Limón-Rocha, I.; Guzmán-González, C.A.; Anaya-Esparza, L.M.; Romero-Toledo, R.; Rico, J.L.; González-Vargas, O.A.; Pérez-Larios, A. Effect of the Precursor on the Synthesis of ZnO and Its Photocatalytic Activity. *Inorganics* **2022**, *10*, 16. [CrossRef]
26. Corbella, C.; Vives, M.; Pinyol, A.; Porqueras, I.; Person, C.; Bertran, E. Influence of the porosity of RF sputtered Ta_2O_5 thin films ontheir optical properties for electrochromic applications. *Solid State Ion.* **2003**, *165*, 15. [CrossRef]
27. Liu, X.; Zhang, J.; Wang, S. Experimental and theoretical band alignment of Ta_2O_5/ZnO stack for heterostructured devices applications. *Phys. B Condens. Matter* **2021**, *612*, 412769. [CrossRef]
28. Bright, T.J.; Watjen, J.I.; Zhang, Z.; Muratore, C.; Voevodin, A.A.; Koukis, D.I.; Tanner, D.B.; Arenas, D.J. Infrared Optical Properties of Amorphous and Nanocrystalline Ta_2O_5 Thin Films. *J. Appl. Phys.* **2013**, *114*, 083515. [CrossRef]
29. Băilă, D.-I.; Vițelaru, C.; Trușcă, R.; Constantin, L.R.; Păcurar, A.; Parau, C.A.; Păcurar, R. Thin Films Deposition of Ta_2O_5 and ZnO by E-Gun Technology on Co-Cr Alloy Manufactured by Direct Metal Laser Sintering. *Materials* **2021**, *14*, 3666. [CrossRef] [PubMed]
30. Băilă, D.-I.; Tonoiu, S. Thin films deposition on 304L stainless steel using e-gun technology for medical applications. *IOP Conf. Ser. Mater. Sci. Eng.* **2019**, *591*, 012001. [CrossRef]
31. Chen, X.; Bai, R.; Huang, M. Optical properties of amorphous Ta_2O_5 thin films deposited by RF magnetron sputtering. *Opt. Mater.* **2019**, *97*, 109404. [CrossRef]

32. Girija, K.G.; Shaheera, M.; Somasundaram, K. Correlating the properties of RF sputtered ZnO nanocrystalline films deposited using sintered and powder targets. *Nano-Struct. Nano-Objects* **2021**, *26*, 100758. [CrossRef]
33. Krishnan, R.R.; Vinodkumar, R.; Rajan, G.; Gopchandran, K.G.; Mahadevan Pillai, V.P. Structural, optical, and morphological properties of laser ablated ZnO doped Ta_2O_5 films. *Mater. Sci. Eng.* **2010**, *174*, 150. [CrossRef]